Hodgkin-Huxley type modelling and parameter estimation of GnRH neurons

Dávid Csercsik [a,c,*], Imre Farkas [b], Gábor Szederkényi [a,c],

Erik Hrabovszky [b], Zsolt Liposits [b,c], Katalin M. Hangos [a],

[a]*Process Control Research Group,*

Computer and Automation Research Institute, Hungarian Academy of Sciences

H-1518, P.O. Box 63, Budapest, Hungary

Tel: +36 1 279 6000

Fax: +36 1 466 7503

[b]*Department of Endocrine Neurobiology*

Institute of Experimental Medicine, Hungarian Academy of Sciences

H-1450 Budapest, P.O. Box 67, Hungary

Tel: +36 1 210 9943

Fax: +36 1 210 9944

[c]*Faculty of Information Technology*

Pázmány Péter Catholic University,

H-1364 Budapest 4., P.O. Box 178 , Hungary

Tel: +36 1 886 47 00

Fax: +36 1 886 47 24

Abstract

In this paper a simple one compartment Hodgkin-Huxley type electrophysiological model of GnRH neurons is presented, that is able to reasonably reproduce the most important qualitative features of the firing pattern, such as baseline potential, depolarization amplitudes, sub-baseline hyperpolarization phenomenon and average firing frequency in response to excitatory current. In addition, the same model provides an acceptable numerical fit of voltage clamp (VC) measurement results. The parameters of the model have been estimated using averaged VC traces, and characteristic values of measured current clamp traces originating from GnRH neurons in hypothalamic slices. The resulting parameter values show a good agreement with literature data in most of the cases. Applying parametric changes, which lead to the increase of baseline potential and enhance cell excitability, the model becomes capable of bursting. The effects of various parameters to burst length have been analyzed by simulation.

Key words: Hodgkin-Huxley type models, GnRH neuron, neuroendocrinology, parameter estimation

1 Introduction

Central control of reproduction in vertebrates is governed by a neuronal pulse generator that controls the activity of hypothalamic neuroendocrine cells secreting

* Corresponding author.
  Email addresses: `csercsik@scl.sztaki.hu` (Dávid Csercsik), `farkas@koki.hu` (Imre Farkas), `szeder@scl.sztaki.hu` (Gábor Szederkényi), `hrabovszky@koki.hu` (Erik Hrabovszky), `liposits@koki.hu` (Zsolt Liposits), `hangos@scl.sztaki.hu` (Katalin M. Hangos).

Gonadotropin-releasing hormone (GnRH). The pulsatile release of GnRH, which is closely associated with concurrent increases in multiunit electrical activity in the mediobasal hypothalamus (Knobil, 1980, 1988; Williams et al., 1990; Wilson et al., 1984; Conn and Freeman, 2000), is driven by the intrinsic activity of GnRH neurons, characterized by bursts and prolonged episodes of repetitive action potentials correlated with oscillatory increases in intracellular Ca^{2+} (Constantin and Charles, 1999, 2001).

In close relation with this, several in vitro experiments have shown that changes in cytosolic Ca^{2+} concentration determine the secretory pattern of GnRH (Stojilkovic et al., 1994), underlining that Ca^{2+} plays a central role in the signal transduction processes that lead to exocytosis. Furthermore, GnRH secretion from perifused GT1 and hypothalamic cells is reduced by L-type Ca^{2+} channel inhibitors and augmented by activation of voltage-gated Ca^{2+} channels (Krsmanovic et al., 1992).

The models of GnRH pulse generator, which can be found in literature nowadays, use very simple generalized neuron models and networks. Furthermore, they are neither based on the known membrane properties of GnRH neurons, nor are able to describe the effect of gonadal hormones (Brown et al., 1994). Nevertheless, these investigations can provide novel results about pulsatility and synchronization (Gordan et al., 1998; Khadra and Li, 2006).

To increase the clinical relevance of the dynamic GnRH models, one has to use sub-models based on as up-to-date biological information as available, and reduce the role of empirical and phenomenological approaches everywhere the biological knowledge makes it possible. In the field of computational neuroendocrinology, in addition to GnRH related topics, good examples of this approach are the articles of

Komendantov et al. (2007) and Roper et al. (2003), which address magnocellular neurosecretory cells.

The general aim of this work is to construct a simple dynamic model of a GnRH neuron that reproduces some of its characteristic properties (see section 2) and the parameters of which can be determined from measurements.

1.1 General electrophysiology and modelling of GnRH neurons

With the application of cell marking based on the green fluorescent protein (GFP) and transgenic mice, the targeted measurements and electrophysiological experiments on GnRH neurons became available (Herbison et al., 2001; Suter et al., 2000). Another possibility for gaining measured data is the application of so called "immortalized" GnRH neurons (Mellon et al., 1990; Wetsel et al., 1992). Since these methods became widespread, the electrophysiological features of this important neuroendocrine cell have been studied extensively both experimentally and by constructing mathematical models to explain the underlying mechanisms of their properties.

Sim et al. (2001) have classified GnRH neurons in intact female adult mice as belonging to four distinct types. Herbison et al. (2001) have characterized the basic membrane properties of GnRH neurons. As mentioned in his article (Herbison et al., 2001), none of the GnRH neuron types seems to express specific electrophysiological 'fingerprint' in terms of the types of the expressed ion channels. However several recordings have demonstrated significant heterogeneity in the basic membrane properties of GnRH neurons (Spergel et al., 1999; Suter et al., 2000) which points to functional heterogeneity. Furthermore, the dynamics of GnRH neurons

4

are affected by peripherial hormones including estradiol (E_2) (DeFazio and Moenter, 2002; Maurer et al., 1999; Farkas et al., 2007; Herbison, 2008; Chu et al., 2009) and progesterone (P_4) (Karsch et al., 1987; Chabbert-Buffet et al., 2000).

Based mainly on data collected from immortalized GT1 cells, a couple of mathematical models (LeBeau et al., 2000; Van Goor et al., 2000; Fletcher and Li, 2009) have been proposed to explain some of the observed experimental results. These models focus mainly on the autocrine regulation by GnRH through adenylyl cyclase and calcium coupled pathways (Helmreich and Bakardjieva, 1980).

However, the firing pattern of GT1 cells and that of the models published in these articles is qualitatively different compared to GFP-tagged GnRH neurons originating from hypothalamic slices. The depolarization, hyperpolarization amplitudes and the spontaneous firing frequency are much lower in the case of GT1 cells (compare eg. the data published in (Van Goor et al., 1999a,b; LeBeau et al., 2000; Van Goor et al., 2000) and (Sim et al., 2001; Chu and Moenter, 2006; DeFazio and Moenter, 2002)). This implies that while these models can be appropriate for analyzing the mechanism of action corresponding to GnRH and various drugs which act through Ca^{2+} coupled pathways, they may be inadequate when the aim is to describe the in vivo behavior of GnRH neurons and the GnRH pulse generator network. Furthermore these models do not include the A-type potassium current, which is shown to be present in GnRH neurons (Kusano et al., 1995; Constantin and Charles, 2001; Sim et al., 2001; Bosama, 1993; Herbison et al., 2001) and is affected by the ovarian hormone estradiol (DeFazio and Moenter, 2002; Farkas et al., 2007), and thus may be a key regulator of neuronal activity during the ovarian cycle.

In order to fulfill the aim of electrophysiological model development, GFP-based

patch clamp recordings were carried out on mouse GnRH neurons (the transgenic mice were available by courtesy of S. Moenter, Univ. of Virginia, Charlottesville, VA, USA). In the present work the obtained data are used to identify a Hodgkin-Huxley type conductance-based model (Hodgkin and Huxley, 1952) of membrane dynamics. The elements of the model (ionic conductances of specific types of ionic channels) were designed using literature data abut the electrophysiological properties of GnRH neurons.

The outline of this paper is as follows; In section 2 the required properties of the model are specified, in section 3 the measurement methods and mathematical modelling are described. Section 4 summarizes the simulation results of the model. Conclusions are drawn in 5. The two appendices describe the details of model equations, the parameter estimation and its results.

2 Model specification

In this section the desired features of the model are defined, and the intended use of the model is explained.

2.1 Characteristic features to be described by the model

The above mentioned experimental observations indicate important characteristic features of GnRH neurons, which should be reproduced by the model. These are as follows.

(1) The model should be able to reproduce the shape of action potentials observed in GnRH neurons originating from hypothalamic slices (Sim et al., 2001; Chu

6

and Moenter, 2006; DeFazio and Moenter, 2002), in particular *the high depolarization amplitudes and the characteristic sub-baseline hyperpolarization after the action potentials (APs).*

(2) The model should exhibit similar *excitability properties* to the cells observed during the measurement process. This means that the same current injection which proved to be able to evoke APs during measurement should have the same effect on the model.

(3) The model should qualitatively reproduce the typical *VC (voltage clamp) traces* of GnRH neurons originating from hypothalamic slices.

(4) The model should be capable of *bursting*. Bursting properties have been described in several articles corresponding to GnRH neurons originating from hypothalamic slices (Kuehl-Kovarik et al., 2005; Suter et al., 2000; Chu et al., 2009) as well as in the case of GT1 cells (Van Goor et al., 1999b; Charles and Hales., 1995). The duration of bursts in GnRH neurons have been found dominantly to range between 1 and 40 s with an average frequency about 10 Hz.

2.2   Intended use of the model

Several mathematical models can be found which aim at describing the hormone levels during the menstrual cycle (Bogumil et al., 1972; Grigoliene and Svitra, 2000; Harris, 2001; Harris et al., 2006; Reinecke and Deuflhard, 2007). The GnRH pulse generator in these models is taken into account (if it is taken into account at all) in a rather simplified way. A more detailed, neurophysiologically relevant model of the GnRH pulse generator network, which is based on up-to-date biological knowledge, would surely improve the clinical significance of such models.

7

The model to be developed should be able to reproduce the dynamic properties of GnRH neurons relevant from the point of view of the female neuroendocrine cycle. Furthermore it should be used as an element of a hierarchical model of the GnRH pulse generator that responds to the ovarian hormone levels and the excitation delivered by neighboring anatomical areas, and is able to capture the main qualitative features of GnRH release in different phases of the ovarian cycle. A further intended aim of this network model will be to analyze the synchronization phenomena (Di Garbo et al., 2007) between GnRH neurons.

3   Methods

The measurement conditions and result are briefly described in this section together with the structure of the applied mathematical model.

3.1   Electrophysiology

3.1.1   Obtaining and preparing samples

Brains of 60-90 days old male mice were used for obtaining GnRH neurons for measurements. The mouse was decapitated, and the brain was rapidly removed and placed in ice-cold artificial cerebrospinal fluid (ACSF) oxygenated with 95% O_2-5% CO_2 mixture. Brains were blocked and glued to the chilled stage of a Leica VT1000s vibratome, and 250-micrometer-thick coronal slices containing the medial septum through to the preoptic area were cut. The slices were then incubated at room temperature for 1 hour in oxygenated ACSF consisting of (in mM): 135 NaCl, 3.5 KCl, 26 $NaHCO_3$, 10 D-glucose, 1.25 NaH_2PO_4, 1.2 $MgSO_4$, 2.5 $CaCl_2$., pH 7.3.

3.1.2 *Whole-cell recording of GnRH neurons*

Slices were transferred to the recording chamber, held submerged, and continuously super-fused with oxygenized ACSF. All recordings were made at 33°C.

In order to visualize GnRH neurons in the brain slices, GnRH-enhanced green fluorescent protein (GnRH-GFP) transgenic mice (kind gift by Dr. Suzanne Moenter) were chosen in which the GnRH promoter drives selective GFP expression in the majority of GnRH neurons. GnRH-GFP neurons were identified in the acute brain slices by their green fluorescence, typical fusiform shape and apparent topographic location in the preoptic area and medial septum.

The electrodes were filled with intracellular solution (in mM): 140 KCl, 10 HEPES, 5 EGTA, 0.1 $CaCl_2$, 4 MgATP, 0.4 NaATP, pH 7.3 with NaOH. Resistance of patch electrodes was 2-3 MΩ. Holding potential was -70 mV, near the average resting potential of the GnRH cells. Pipette offset potential, series resistance and capacitance were compensated before recording.

The protocol for voltage clamp (VC) recordings was the following: twelve voltage steps were applied starting from the holding potential. The first step was -40mV and the subsequent steps were increased by 10 mV. Duration of the steps was 30 ms, starting at 10 ms. During the voltage clamp measurements with prepulse, a -100 mV prepulse was applied just preceding the voltage steps (from 0.8 to 10 ms) with a duration of 9.2 ms.

The protocol for current clamp (CC) recordings to activate action potentials (APs) was: the holding current was 0 pA. First the resting potential was measured then current step of 10 pA for 200 ms was applied to the cells. If the 10 pA current failed to evoke APs, it was elevated by 10 pA steps till it induced 3-4 APs.

3.2   Measurement results

Overall 5 cells have been investigated by performing voltage clamp (VC) and current clamp (CC) measurements.

3.2.1   Voltage clamp

VC traces without prepulse have been recorded in the case of all cells, and voltage clamp recordings with prepulse have been completed in the case of one cell (No. 2).
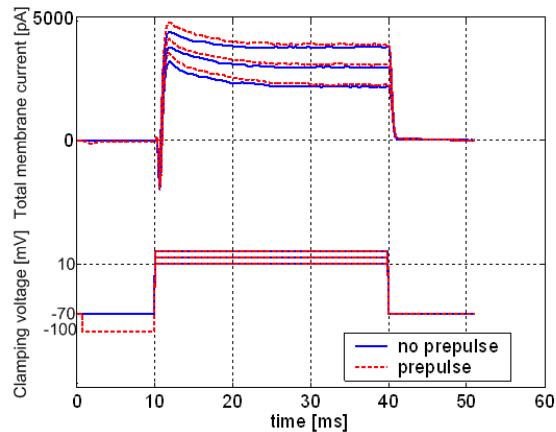

Fig. 1. Comparison of VC traces (step to 10 20 30mV from -70 mV) without and with prepulse in the case of cell No.2. The prepulse facilitates the recovery from inactivation in the case of the fast A-type potassium current, and also influences slower currents. Down: Voltage clamp waveforms

Fig. 1 clearly indicates that the application of prepulse facilitates the recovery of the inactivation variable of the fast A-type current and increases it's amplitude. It is worth to observe that the application of prepulse also affects the sustained component of the outward current.

10

Since measurement data of several cells were available, but VC traces with prepulse were not recorded in all of the cases, the averaged VC traces without prepulse were used as basis for parameter estimation procedure. Voltage clamp traces with prepulse were used to validate the resulting model, by comparison of the measured and simulated effects of prepulse to VC traces.

3.2.2   Current clamp

Regarding the current clamp (CC) measurements, various amplitude depolarizing injected current steps were needed to elevate APs. The 30 pA traces of the cells are depicted in Fig. 2.
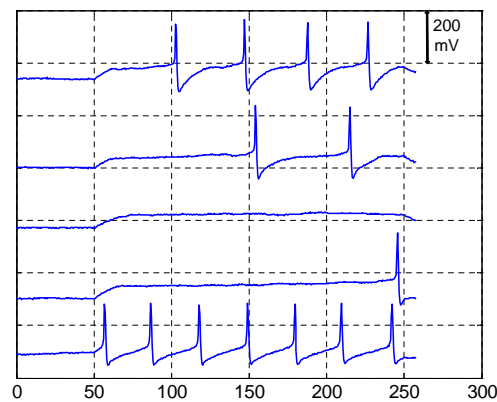

Fig. 2. The 30 pA current clamp (CC) traces of the cells 1-5 (from up to down). The resting potential values of the cells were: -71, -69.2, -73, -79, and -53 mV.

3.3   Mathematical model and its parameter estimation

The simplest possible single compartment model of GnRH neurons is described in this section, which is able to fulfill the modelling goals stated in section 2.1. For the sake of simplicity we do not include the changes of intracellular Ca^{2+}

11

concentration and calcium dependent currents in the model. As a consequence we assume a constant reversal potential of Ca^{2+}.

3.3.1 Elements of the model

The elements of the model are presented in terms of ionic channels that are taken into account.

- The presence of tetrodotoxin-sensitive *Na^+ currents* has been experimentally confirmed in the case of GT1 cells (Bosama, 1993) and embryonic GnRH neurons (Kusano et al., 1995). Adult GnRH neurons were found to fire Na^+ dependent action potentials (Sim et al., 2001). The sodium current in the model will be denoted by I_{Na}. We suppose third order activation and second order inactivation dynamics.

- The presence of *A-type K^+ transient or rapidly activating/ inactivating conductance* has been described in the case of GT1 cells (Bosama, 1993; Constantin and Charles, 2001), in embryonic cultures (Kusano et al., 1995), and in GnRH neurons originating from mice (Sim et al., 2001; Herbison et al., 2001). This current will be denoted by I_A in the model. This type of potassium current is quite widely studied in the literature even in the case of GnRH neurons (DeFazio and Moenter, 2002), and on hypothalamic neurons in general (Wang et al., 1997; Luther and Tasker, 2000). These results provide useful initial values for the parameters of this current. Furthermore, literature data indicated that the ovarian hormone estradiol modulates this current in mice GnRH neurons (DeFazio and Moenter, 2002) and also in GT1 cells (Farkas et al., 2007).

- A voltage gated *delayed outward rectifier K^+ channel* can be assumed, which contributes to the more slowly activating, sustained component of the outward

K^+ current (I_K) - see (Kusano et al., 1995; Constantin and Charles, 2001; Sim et al., 2001; Bosama, 1993; Herbison et al., 2001).

- A *non-inactivating M-type K^+ current (I_M)* is also taken into account, which is considered a key modulator of neuronal activity in GnRH cells (Xu et al., 2007).

As stated before, the main perspective of this modeling procedure is the description of GnRH release. Based on the results that underline the importance of calcium oscillations corresponding to hormone release (Stojilkovic et al., 1994; Krsmanovic et al., 1992), we take 3 types of Ca^{2+} conductance into account to be able to describe the qualitatively different components of the calcium current.

Furthermore, according to the results of Beurrier et al. (1999), the interplay of different calcium currents can contribute to periodic bursting behavior which can be of high importance regarding neuroendocrine functions.

- *Low voltage activated (LVA) T-type* Ca^{2+} conductance, which is activated in earlier phases of depolarization (I_T), has been described in the case of rat (Kato et al., 2003) and mouse GnRH neurons (Herbison et al., 2001), as well as in GT1 cells (Van Goor et al., 1999a).

- Furthermore, based on the results of Watanabe et al. (2004) related to GT1-7 cells, and in vitro experiments (Kato et al., 2003; Nunemaker et al., 2003), we assume a *high voltage gated (HVA) Ca^{2+} channel* representing *R and N type conductances* (I_R)

- In addition, a *HVA long-lasting current (L-type) Ca^{2+} channel* is modelled (I_L) - see Krsmanovic et al. (1992); Nunemaker et al. (2003) for in vitro results and Van Goor et al. (1999a) for GT1 measurements.

13

- Lastly, two *leakage currents* corresponding to *sodium* (I_{leakNa}) and *potassium* (I_{leakK}) with constant conductance are taken into account.

Several other ionic currents have been shown to appear in GnRH neurons, for example the $I_{Q/H}$ current (Sim et al., 2001), Ca^{2+} activated potassium currents (Chu and Moenter, 2006; Fletcher and Li, 2009), which are not considered in the model. The reason for this is that the further (especially Ca^{2+} dependent) currents would significantly increase the model complexity, which would lead to a smuch harder solvability of the parameter estimation problem. Furthermore these currents turned out to be nonessential for the reproduction of the features determined in section 2.1. After a simple model has been identified it can easily be extended with the currents omitted in the first step of the modelling process, if needed.

3.3.2   Model Equations and Parameters

The **equivalent electric circuit** of a one-compartment GnRH neuron model with all the above conductances is shown in Fig, 3.
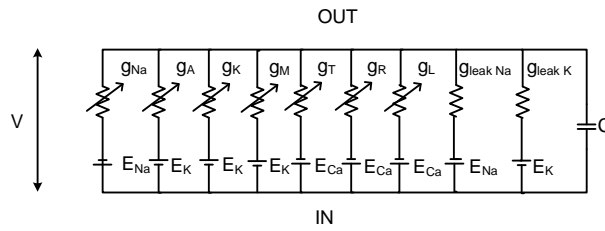

Fig. 3. Parallel conductance model, with conductances representing different ion channels in voltage dependent and independent manner. g_{Na} denotes the sodium conductance, g_A, g_K and g_M denote the A-type, delayed rectifier and M-type potassium conductances, g_T, g_R and g_L stand for the conductances related to T-type LVA and the R and L-type HVA calcium currents, g_{leakNa} and g_{leakK} correspond to the voltage independent leakage currents.

14

The voltage (V), which is the observed output of the system in current clamp mode, is described by

$$\frac{dV}{dt} = -\frac{1}{C}(I_{Na} + I_A + I_K + I_M + I_T + I_R + I_L + I_{leakNa} + I_{leakK}) + \frac{1}{C}I_{ex} \qquad (1)$$

where C is the membrane capacitance, I_i are the currents of the ionic channels considered, i.e. the Na^+, the three types of K^+ (A,K,M), the three types of Ca^{2+} (T,R,L) and two types of leakage currents (leakNa, leakK), while I_{ex} is the external (injected) current. Each ionic channel current is a function of an activation m_i and an inactivation h_i variable in the form of

$$I_i = \bar{g}_i m_i^{\gamma_i} h_i^{\mu_i}(V - E_x) \qquad (2)$$

(except the M type K^+ current that inhibits no inactivation dynamics). In Eq. 2 $\bar{g}_i$ denotes the maximal conductance, γ_i and μ_i are positive integers, and E_x is the reversal potential of the corresponding ion ($x \in Na, K, Ca$). γ_i, μ_i, and the reversal potentials are assumed to be known. The detailed equations describing the time variation of m_i and h_i are given in section 7.1 of Appendix B.

The unknown model parameters to be estimated are the membrane capacitance C in (1), the maximal conductances $\bar{g}_i$ in 6 and the activation/inactivation parameters in (5) in section 7.1. All together we have to estimate 1+9+6*12+6 = 88 parameters.

3.3.3 Parameter estimation

The parameter estimation problem of neuronal models is a widely studied area in neuroscience literature. The diversity of models, however, implies a broad range of approaches and solutions that are sometimes difficult to apply for other types of

15

neurons or estimation tasks. The same applies for the parameter values of various ionic channels that are reported in the literature. These parameter values are found to be different depending on the type of cells on which the ionic channels are operating, and they may even depend on the actual functioning of a particular cell type.

In addition, regarding membrane properties, GnRH neurons form a heterogenous population (Sim et al., 2001), which implies that cells with different functionality may be described by models with the same model structure, but significantly different parameters.

Furthermore, the complex bifurcation structure of Hodgkin-Huxley (HH) type models implies that even a slight variation of these parameters may cause significant deviances in the model behavior. As a consequence, to reproduce an observed firing pattern or excitability level, one has to carry out a parameter estimation procedure of the applied model. An algorithmic identification process, which takes into account the most available measurement data, can significantly improve the reliability and performance of the model.

The basic articles, which describe the parameter estimation of HH type models have been published by Tabak et al. (2000) and Willms et al. (1999). The article of Lee et al. (2006) analyzes the effect of simplifying assumptions on the results of parameter estimation, and provides a promising problem-reformulation based numerical method in the case of VC measurements. Haufler et al. (2007) describe a synchronization-based method based on CC measurements. The interesting paper of Tien and Guckenheimer (2008) focuses on bursting neural models and uses a geometric approach. The paper of Huys et al. (2006) provides a statistical method for the parameter estimation of multicompartmental models. Despite the existence

16

of the above valuable work, however, there is a lack of mathematically and algo-rithmically well founded parameter estimation method for neuronal models, that is able to take into account both the qualitative and quantitative aspects of measured data.

In our case, a multistep recursive parameter estimation approach has been applied that consists of the following steps:

(1) Initialization of model parameters, based on literature data and intuitive heuris-tic considerations based on CC traces

(2) Parameter estimation by optimization based on VC and CC traces

(3) Model verification and validation

The main aim of these considerations was to avoid local minimum points of the ob-jective functions and to reproduce those qualitative features of the model behavior, which inhibit significant physiological importance, and, according to our obser-vations, can not be captured well by the numerical optimization methods. These features were the sharp action potentials and partially the significant hyperpolar-izations after the APs.

The *intuitive tuning and initialization of model parameters* was based on decom-position of the CC trace. The considered parts of the CC trace are shown in Fig 4. From different parts of the CC trace, the initial values of different parameters were roughly estimated as follows.

- Our simulation studies show that the *resting potential* is mainly determined by the potassium and the low threshold Ca (g_T) conductances, their steady-state parameters (m_∞, h_∞) and the leak conductances.

- *Injected current-induced depolarization* is dominantly influenced by the 3 potas-
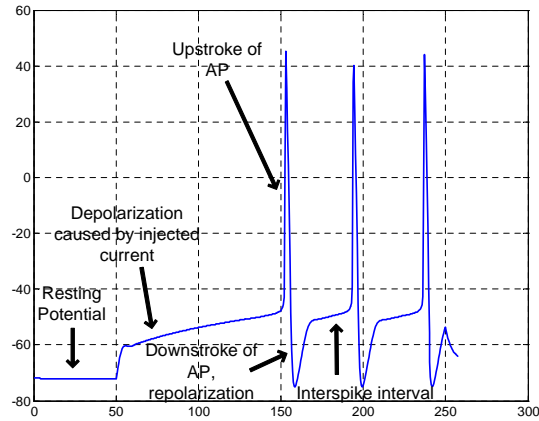
Fig. 4. Membrane potential during CC (30 pA) - simulation of the model resulting from parameter estimation. The number and shape of APs show also good agreement with measurement results.

sium currents, the T-type calcium current, and in minor part by the leak currents.

- *Upstroke of AP* is influenced by *Na* and R and L-type *Ca* currents.

- *Downstroke of AP* and hyperpolarization is determined mainly by K^+ currents, especially by the recovery of A-type current from inactivation.

- Finally, the *interspike intervals* are influenced by delayed rectifier and M-type potassium currents, low threshold T-type calcium and partially by A-type potassium and leak currents.

Regarding the *optimization based parameter estimation*, to increase the validity of the model, our approach was to take both voltage and current clamp traces into account. The algorithmic part of the parameter estimation procedure minimizes an objective function that is a function of the parameters to be estimated, i.e. an optimization-based estimation procedure is used (Hough et al., 2000). A brief description of the optimization procedure used in the parameter estimation can be found in appendix A. Earlier results corresponding to the parameter estimation of

18

GnRH neurons are described in (Csercsik et al., 2009a,b).

4   Results and Discussion

The parameter set, which reproduced the most important qualitative features of the firing patterns, and also provided a good fit of VC traces, has been obtained using the multistep process described above in section 3.3.3, iterating steps (1) and (2). The estimated model parameters can be found in subsection 7.2 of Appendix B.

If we compare the results with literature data, we can make the following observations.

- The activation and inactivation curves of the A-type K^+ current in the model show reasonable agreement with the results published by DeFazio and Moenter (2002). Furthermore, the voltage-dependence characteristics of the activation time constant of τ_{mA} of I_A in higher voltage ranges (above 0 mV) are in good agreement with the results of Luther and Tasker (2000) regarding hypothalamic cells. In the lower voltage ranges the activation time constant published in Luther and Tasker (2000) exceeds that our model by 1-4 ms. The inactivation time constants of the model show significant difference (20-30 ms) in the lower voltage ranges (about -40 mV) compared to this article.

- The activation and inactivation curves of R-type Ca^{2+} current are in good agreement with the results of Kato et al. (2003). The amplitude of Ca^{2+} currents in the case of VC simulations is similar to measurement results of Kato et al. (2003).

- The characteristics of the T-type LVA Ca^{2+} current are in good agreement with the results of Talavera and Nilius (2006).

19

4.1   Current clamp results

It should be noted that the model parameters were estimated using both VC and CC traces, while CC measurements were only available for one current step value (30 pA). The simulated CC trace in response to a 30 pA current step is depicted in Fig. 4.

In contrast to the VC traces where the simulated responses were compared to the average measured responses, in the case of CC traces the characteristic features of the measured and simulated CC traces were compared. The characteristic values (number of APs, depolarization and hyperpolarization values) of the simulated CC trace are compared with the average values corresponding to the measured CC traces (depicted in Fig. 2) in Table 1.

Table 1

Average characteristic values of measured (meas) CC traces, and characteristic values of the simulated (sim) CC trace in response to 30 pA: resting potential (RP), number of APs (APs), depolarization value (DP), hyperpolarization value (HP).

	RP	APs	DP	HP
meas	-69.05	2.8	43.25	-86.75
sim	-72.1	3	42.93	-75.03

The results show that the model can reasonably capture the excitability properties of the GnRH neuron in this case of injected current. The resting potential, the number of APs, the average depolarization amplitude, and the average time between the

APs in the simulation results show also good agreement with measurement data.

On the other hand, while the model reproduces the characteristic sub-baseline hyperpolarization, it can not describe the hyperpolarization amplitudes well. The reason for this may be the lack of Ca^{2+} activated K^+ channels, however it is stated in (Van Goor et al., 2000) that $[Ca^{2+}]_i$ levels reached during spontaneous AP firing are not sufficient to activate large and small conductance Ca^{2+}-activated K^+ channels. In the case of bursting these channels could possibly improve the description of sub baseline hyperpolarization.

The simulations also showed, that hyperpolarization is determined dominantly by the delayed rectifier K-type and non-inactivating M-type K^+ currents, and by the recovery of A-type K^+ current from inactivation. Furthermore the deactivation and inactivation of high voltage activated Ca^{2+} currents, as well as that of the Na^+ current turned out to be essential for the sub-baseline hyperpolarization. The higher powers of the activation variables of fast Ca^{2+} currents - similar to the model published by Fletcher and Li (2009) - facilitates this fast deactivation.
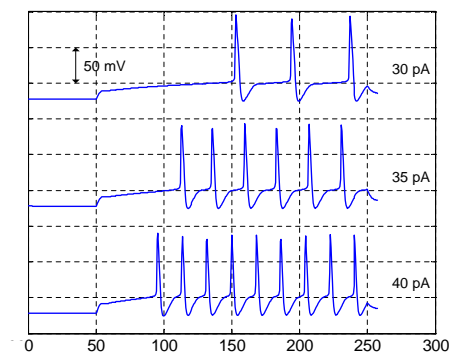

Fig. 5. Simulated CC traces in the case of various amplitude injected currents. The current injection starts at 50 ms and ends at 250 ms. The model reproduces the increase in firing frequency in response to the increase in injected current. The resting potential is about -72mV.

Furthermore, as one increases the injected current in the simulations, the firing frequency increases (see Fig. 5), as it could be observed in CC measurements.

4.2 Voltage clamp results

In Figs. 6-7 the comparison of the averaged VC traces and the model simulations can be seen. The holding potential was -70 mV.
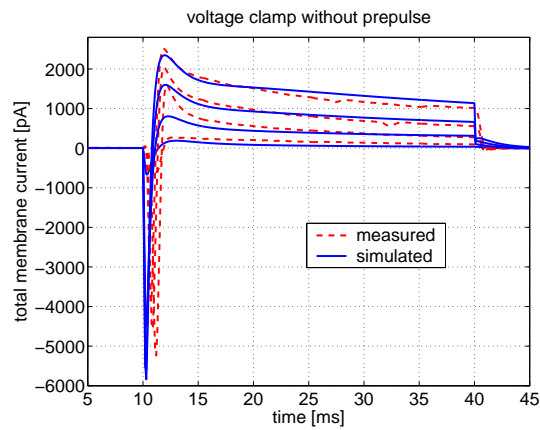

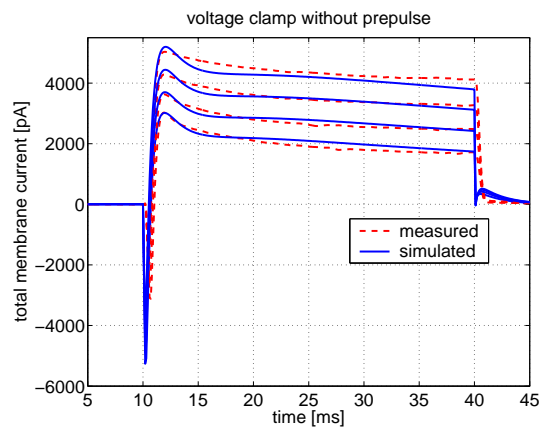Fig. 6. Measured and simulated VC traces corresponding to voltage steps of -40, -30, -20 and -10 mV.

Fig. 7. Measured and simulated VC traces corresponding to voltage steps of 0, 10 and 20 mV.

As it can be seen in Figs. 6 and 7, regarding voltage clamp, the model performs

better in the medium and high voltage ranges. The steady-state and pre-steady state currents are well fit, and the dynamics of the transient currents are quite reasonably captured in the case of approximately half of the traces. Furthermore, in some cases, after the end of the voltage step, at 40 ms, significant tail currents appear in the simulations, which are not confirmed by measurement results.

4.2.1   Effect of prepulse

Because VC measurements with prepulse were not available for all of the cells, the prepulse VC data were not used for the parameter estimation process. Instead, these measurements were used for model validation. In Fig. 8, where the prepulse response of the model is depicted, it can be seen that the effect of prepulse on the model is qualitatively the same as observed in the case of cell 2 depicted in Fig 1: it moderately enhances the recovery of the A-type current, and in general it increases the amplitude of the outward K^+ current. Furthermore the quantitative degree of the increase is approximately the same as observed in measurements (see Fig. 1).
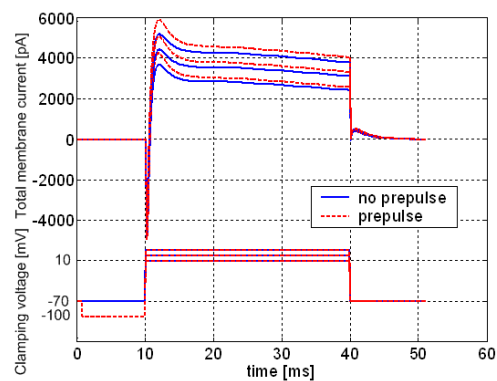

Fig. 8. Simulated VC traces with and without prepulse in the case of 10, 20 and 30 mV voltage steps. Down: voltage clamp waveforms.

4.3 Bursting properties of the model

As it is described in (Constantin and Charles, 1999, 2001), bursts and prolonged episodes of repetitive action potentials contribute to oscillatory increases in intracellular Ca^{2+}, which determine the secretory pattern of GnRH (Stojilkovic et al., 1994).

Several results support the hypothesis, that bursts in GnRH neurons are connected with depolarizing afterpotentials (DAPs) (Kuehl-Kovarik et al., 2005). The results of Chu and Moenter (2006) show that these slow DAPs are connected with TTX dependent sodium conductances.

As it has been described in section 2.1, our aim was to create a model which is able to describe bursting. The resting potential of the basic model, which showed no bursting properties, was about -70 mV as depicted in Fig. 4. As described by Suter et al. (2000), the average resting potential of GnRH neurons that generated bursts was about -60 mV. This data served as a basic guideline in the task of parameter modification to achieve bursting. The basic parameter set of the bursting model is described in Tables 4 and 5 of subsection 7.3 in Appendix B.

In the simulations a 2 ms wide 100 pA pulse was applied at 50 ms to evoke bursting. The simulation result of the basic bursting model is depicted as the first trace in Fig. 10.

Furthermore we have to note, that the average firing frequency in the burst simulations ranged from 33 to 40 Hz, which is higher compared to the burst frequency described in (Suter et al., 2000) and (Kuehl-Kovarik et al., 2005). In general it can be stated that the bursting of the model is quite sensitive to parametric changes, and

bursting can be easily terminated or turned into a continual firing pattern.

4.3.1 Dependence on T-type Ca^{2+} current

The sodium conductance of the model is not able to reproduce 400-600 ms DAPs as described in (Kuehl-Kovarik et al., 2005) according to the observed simulation results. However, the T-type Ca^{2+} current in the model, which inhibits slow deactivation features, and interacts with the A-type current during after-hyperpolarization, can produce short depolarizing oscillations following the APs, which can serve as basis for bursting.

Reducing the maximal conductance of this current can cause the abrupt termination of bursting, as depicted in Fig. 9. These simulation results indicate that the model predicts a possible mechanism of bursting, which is based on T-type Ca^{2+} currents. This hypothesis of course requires further experiments for validation.
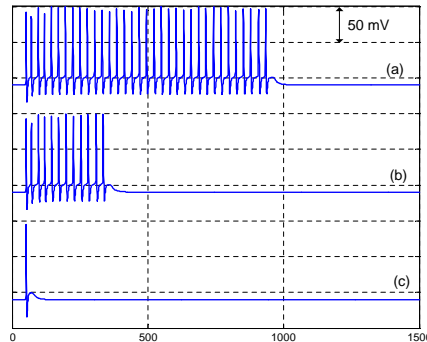

Fig. 9. Reducing the T-type Ca^{2+} current ($\bar{g}_T = 10.79$ nS) leads to the shortening of burst length (*b*) compared to basic burst simulation (*a*) ($\bar{g}_T = 10.8$ nS). Further reduction of $\bar{g}_T$ (10.2 nS) leads to the termination of bursting (*c*). The depolarizing wave after the AP can still be observed in this case. The baseline potential was about -60 mV

25

4.3.2 Influence of the Ca^{2+} currents on the length of burst

Model simulations show that not only T-type, but other Ca^{2+} currents influence the bursting behavior. If we decrease the R-type Ca^{2+} conductance of the model by 0.02 nS, the length of the burst decreases (compared to the first trace of Fig. 9), as it can be seen in the first trace in Fig. 10. Increasing this conductance (by 0.01 nS) implies an opposite effect, as depicted in the second trace of Fig. 10.

The L-type Ca^{2+} conductance affects bursting in the opposite way. If the conductance is decreased the length of the burst increases, and vice versa.
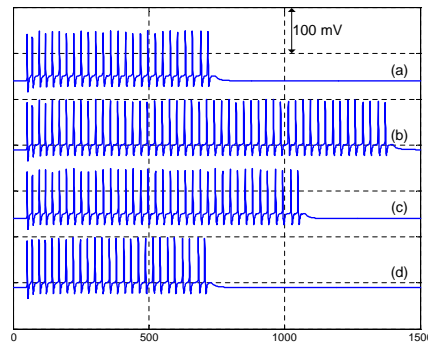
Fig. 10. The R-type Ca^{2+} conductance enhances the burst length: (*a*) $\bar{g}_R = 10.83nS$, (*b*) $\bar{g}_R = 10.86nS$. The L-type conductance shows an opposite effect: If the conductance is decreased ($\bar{g}_L = 13nS$), the burst length increases (*c*), and if the conductance is increased ($\bar{g}_L = 15nS$) , the burst length decreases (*d*).

The modulating effect of the L-type Ca^{2+} current in the model simulations is an interesting result, which can be the subject of further simulation and experimental studies.

4.3.3 Influence of the K^+ currents on the length of burst

Farkas et al. (2007) analyzed the effect of estrogen in the case of GT1 cells, and

26

found that estrogen modulates (increases) the expression of the Kv4.2 subunit, which contributes to the function of the A-type K^+ channels. This might be interpreted as an increase in the parameter $\bar{g}_A$. We can see in Fig. 11 that the maximal conductance of the fast A-type K^+ current is able to control the length of the bursts in the case of this parametrization. In the case of trace (a), $\bar{g}_A$ was increased to $375.1nS$, which reduced the burst length.
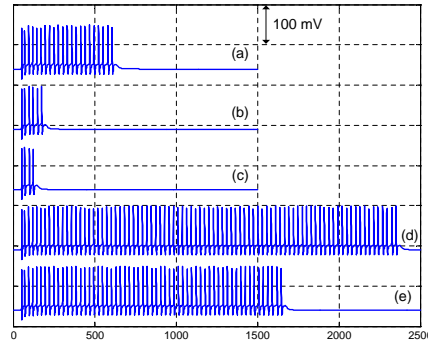

Fig. 11. (a) increase of $\bar{g}_A$ from 375 to 375.1 nS reduces the burst length. (b) change of $V_{1/2}$ of m_∞ of the A-type current to -33.22 from -33.2 and increasing the $V_{1/2}$ parameter of h_∞ curve (c) from -61.5 mV to -61.47 mV acts in a similar fashion. (d) Decrease of $V_{1/2}$ of h_∞ of the A-type to -61.501 significantly increases the length of the burst. (e) Modulation by M-type current: The reduction of $\bar{g}_M$ from 4.7 mS to 4.69 mS increases burst length.

DeFazio and Moenter (2002) described that estradiol strongly influences the excitability of GnRH neurons in the case of ovariectomized mice. This article also describes that estrogen significantly affects the inactivation characteristics of A-type K^+ current, by depolarizing the voltage at which the current inactivates. The activation curve is also affected but in a less serious fashion.

With the proposed model one is able to test whether the increased cell excitability (which should lead to increased bursting activity) can be caused by these effects of estrogen on activation curves of the A-type K^+ current.

27

In trace (*b*) of Fig. 11 we can see, that shifting the activation curve of the A-type K$^+$ current to the left (by decreasing the $V_{1/2}$ parameter of the steady state curve by 0.02 mV) decreases the length of the burst. Trace (*c*) depicts that increasing the $V_{1/2}$ parameter of the inactivation curve by 0.03 mV has similar effects. In contrast, decreasing the $V_{1/2}$ parameter of the inactivation curve of I_A can lead to significant increase in burst length (trace (*d*) in Fig. 11).

It is likely that the combination of multiple effects of estrogen is necessary to increase cell excitability, and this complex effect can not be captured by manipulating single parameters of the model. For example, the results of Farkas et al. (2007) indicate that estrogen also affects the K-type potassium current.

Finally, the effect of M-type K$^+$ current was analyzed. Decreasing the M-type conductance also increases burst length, as expected (see trace (*e*) in Fig. 11).

In fact, further in silico, in vitro and in vivo experiments are necessary for the reasonable description of estrogen effect on GnRH cell electrophysiology.

5 Conclusions and future work

As the first step of a bottom-up procedure to build a hierarchical model of the GnRH pulse generator, a simple one compartment Hodgkin-Huxley type electrophysiological model of the GnRH neuron was constructed. The parameters of the model were estimated using both VC and CC data originating from cells in hypothalamic slices. The initial values of parameter estimation were determined using literature data and qualitative biological knowledge. The parameter estimation process itself was carried out as a combination of algorithmic (APPS) and manual methods to reproduce the voltage clamp traces and firing pattern observed in the measurement data.

The resulting parameter set provides a good fit in terms of the qualitative features of neuronal behavior (resting potential, excitability, depolarization amplitudes, sub-baseline hyperpolarizations), and an acceptable numerical fit of VC measurement results. Further measurements are planned with specific channel blockers, that would help in further tuning or even re-parametrization of the model.

Applying parametric changes, which lead to the increase of baseline potential and enhance cell excitability, the model becomes capable of bursting. The properties of bursting behavior could be of high impact regarding physiological functions corresponding to hormone release. The bursts experienced in model simulations are dependent on Ca^{2+} currents, and are strongly affected by the parameters of the A-type K^+ current. Further experiments are necessary to test whether this type of bursting can really appear in GnRH neurons, or this phenomenon is an artificial in silico byproduct of the model.

The resulting model may be used as reference in the development of future models for the GnRH neuron. As soon as an appropriate Hodgkin-Huxley type model of membrane dynamics has been identified and validated, it will be completed with further elements influencing intracellular Ca^{2+} dynamics (models of intracellular compartments such as the endoplasmic reticulum, *Ca* buffers (Shorten and Wall, 2000), and *IP*$_3$ signaling (Young and Keizer, 1992; Tien et al., 1996)), which probably exert an important impact on hormone release.

Additionally, the model will be extended to take the complex effects of estradiol on the dynamics of membrane potential into account (Chu et al., 2009).

6   Appendix A: Parameter estimation method

The parameter estimation was carried out using the data averaged for all the 5 cells. The voltage clamp traces could be interpreted without any problem, and the 2-norm based optimization could be applied for the averaged traces. Both voltage and current clamp data was taken into account during the identification process.

Regarding the VC traces, the objective function of the estimation was the standard two-norm of the difference between the measured and simulated output currents in the case of the protocol defined in 3.1.2.

Current clamp traces were taken into account in the way that the model should have had similar firing properties as the average cell population - see Fig. 1. This meant that the average number of APs and the average depolarization and hyperpolarization values of the recorded CC traces in response to 30pA excitatory current were compared to model simulation. The value of 30pA was chosen, because this CC trace was available in the case of all the cells, and in response to this current 4 of the 5 cells fired action potentials.

Numerical optimization was performed by the APPS algorithm (Kolda, 2005), which is an asynchronous extension of the PPS method that efficiently handles situations when the individual objective function evaluations may take significantly different time intervals and therefore it is very suitable to be implemented in a parallel or grid environment. Furthermore, recent implementations of the APPS method handle bound and linear constraints on the parameters. The global convergence of APPS under standard assumptions is also proved by Kolda and Torczon (2004).

7   Appendix B: Model equations and estimated parameters

7.1   The mathematical model

The model depicted in Fig, 3 can be described by the following equations:

$$\frac{dV}{dt} = -\frac{1}{C}(I_{Na} + I_A + I_K + I_M + I_T + I_R + I_L + I_{leakNa} + I_{leakK}) + \frac{1}{C}I_{ex} \tag{3}$$

$$\frac{dm_i}{dt} = (m_{i\infty} - m_i)/\tau_{mi}, \quad \frac{dh_i}{dt} = (h_{i\infty} - h_i)/\tau_{hi} \tag{4}$$

where V is the membrane voltage, C is the membrane capacitance, I_{Na} denotes the sodium current, I_A, I_K and I_M denote the A-type, delayed rectifier and M-type potassium currents, I_T, I_R and I_L stand for the T-type LVA and the R and L-type HVA calcium currents, I_{leakNa} and I_{leakK} for the leakage currents. The m_i and h_i variables are the activation and inactivation variables of the corresponding currents. $m_{i\infty}, h_{i\infty}$ and $\tau_{mi/hi}$ denote the steady-state activation and inactivation functions, and the voltage dependent time constants of activation and inactivation variables, which are nonlinear Boltzmann and Gauss -like functions of the membrane potential:

$$a_{\infty i} = \frac{1}{1 + e^{\frac{V_{1/2_{ai}} - V}{K_{ai}}}}$$

$$a \in \{m, h\}, \quad i \in \{Na, A, K, M, T, R, L\}, \ K_{mi} > 0, K_{hi} < 0 \ \ \forall i$$

$$\tau_{ai} = C_{base_{ai}} + C_{amp_{ai}} \ e^{\frac{-(V_{max_{ai}} - V)^2}{\sigma_{ai}^2}} \tag{5}$$

The M-type current has only activation dynamics.

Finally, I_{ex} refers to the external injected current.

The currents of ionic channels are given by

$$
\begin{aligned}
I_{Na} &= \bar{g}_{Na} m_{Na}^3 h_{Na}^2 (V - E_{Na}), \quad I_A = \bar{g}_A m_A^2 h_A^2 (V - E_K) \\
I_K &= \bar{g}_K m_K h_K (V - E_K), \quad I_M = \bar{g}_M m_K (V - E_K) \\
I_T &= \bar{g}_T m_T h_T (V - E_{Ca}), \quad I_R = \bar{g}_R m_R^2 h_R (V - E_{Ca}) \\
I_L &= \bar{g}_L m_L^2 h_L (V - E_{Ca}) \\
I_{leakNa} &= \bar{g}_{leakNa} (V - E_{Na}), \quad I_{leakK} = \bar{g}_{leakK} (V - E_K)
\end{aligned}
\tag{6}
$$

where the E_{Na}, E_K, E_{Ca} denote the reversal potentials of the corresponding ions.

7.2 Estimated parameters of the basic model

Parameters of the basic model, resulting from the fit to VC traces and average values of CC traces, are described in the following tables.

Table 2

Estimated capacitance and conductance values

C	$\bar{g}_{Na}$	$\bar{g}_A$	$\bar{g}_K$	$\bar{g}_M$
7	170	170	67	7.7

$\bar{g}_T$	$\bar{g}_R$	$\bar{g}_L$	$\bar{g}_{leakNa}$	$\bar{g}_{leakK}$
3.2	10.5	10.4	0.06	0.12

where [C]=pF, [g]=nS

Table 3

Estimated activation and inactivation parameters

variable	$V_{1/2}$	K	V_{max}	σ	C_{amp}	C_{base}
m_{Na}	-38.2	4.5	-43	45	0.04	0.09
h_{Na}	-45	-4	-78	19	25	0.7
m_A	-36.2	10.9	-58	18	0.7	0.9
h_A	-63.5	-6.9	-100	32	24.4	3.4
m_K	-7.2	12.8	-25	40	0.9	2.0
h_K	-67.2	-8	-39	55	-90	103
m_M	-31.4	6.9	25	28	3.1	2.2
m_T	-47	5.5	-22	32	2.2	2.5
h_T	-78	-6.5	-53	22	3.8	4.1
m_R	-4	10.6	20	30	0	0.4
h_R	-37	-11.5	-47	26	22	17
m_L	-2	10.5	26	33	2.3	0.5
h_L	-34	-11.5	-35	49	65	80

where $[V_{1/2}]$=mV, $[V_{max}]$=mV, $[C_{amp}]$=ms, $[C_{base}]$=ms

The reversal potentials (see Eq. (6)) were determined based on the ionic concentrations of the intra and extracellular solutions used during recording, and literature

data. The assumed reversal potentials are:

$$E_{Na} = 100 \ mV, \quad E_K = -94 \ mV, \quad E_{Ca} = 80 \ mV$$

7.3 Parameters of the bursting model

The parameters of the bursting model are described in the following tables. The parameters different from the basic model are emphasized with bold typeface.

Table 4

Modified (in bold) capacitance and conductance values

C	$\bar{g}_{Na}$	$\bar{g}_A$	$\bar{g}_K$	$\bar{g}_M$
7	**190**	**375**	**57**	**4.7**

$\bar{g}_T$	$\bar{g}_R$	$\bar{g}_L$	$\bar{g}_{leakNa}$	$\bar{g}_{leakK}$
10.8	**10.85**	**13.4**	**0.08**	0.12

where [C]=pF, [g]=nS

Table 5

Modified (in bold) activation and inactivation parameters

variable	$V_{1/2}$	K	V_{max}	σ	C_{amp}	C_{base}
m_{Na}	-38.2	**4.51**	-43	45	0.04	0.09
h_{Na}	-45	-4	-78	19	**20**	0.7
m_A	**-32.2**	10.9	**-65**	**23**	**1.7**	0.9
h_A	**-61.5**	-6.9	-100	**19**	**10**	**5.4**
m_K	**-6.5**	12.8	-25	40	0.9	2.0
h_K	**-68.2**	-8	-39	55	-90	103
m_M	**-29.2**	**6.2**	25	28	3.1	2.2
m_T	**-45**	**7.5**	**-42**	32	**3.1**	**3.9**
h_T	**-73**	**-5.5**	**-44**	22	**4.8**	**4.4**
m_R	-4	10.6	-	-	0	0.4
h_R	-37	-11.5	-47	26	22	17
m_L	**-6**	**12**	26	33	2.3	0.5
h_L	-34	-11.5	-35	49	65	80

where $[V_{1/2}]$=mV, $[V_{max}]$=mV, $[C_{amp}]$=ms, $[C_{base}]$=ms

References

Beurrier, C., Congar, P., Bioulac, B., Hammond, C., 1999. Subthalamic nucleus
neurons switch from single-spike activity to burst-firing mode. The Journal of

Neuroscience, 19, 599–609.

Bogumil, R., Ferin, M., Rootenberg, J., Speroff, L., vande Wiele, R., 1972. Mathematical studies of the human menstrual cycle. I. formulation of a mathematical model. Journal of Clinical Endocrinology and Metabolism 35, 126–143.

Bosama, M., 1993. Ion channel properties and episodic activity in isolated immortalized gonadotropin-releasing hormone (GnRH) neurons. Journal of Membrane Biology 136, 85–96.

Brown, D., Herbison, A., Robinson, J., Marrs, R., Leng, G., 1994. Modelling the lutenizing hormone-releasing hormone pulse generator. Neuroscience 63, 869–879.

Chabbert-Buffet, N., Skinnerb, D., Caratyb, A., Boucharda, P., 2000. Neuroendocrine effects of progesterone. Steroids 65, 613–620.

Charles, A., Hales., T., 1995. Mechanisms of spontaneous calcium oscillations and action potentials in immortalized hypothalamic (GT1-7) neurons. Journal of Neurophysiology 73, 56–64.

Chu, Z., Andrade, J., Shupnik, M., Moenter, S., 2009. Differential regulation of gonadotropin-releasing hormone neuron activity and membrane properties by acutely applied estradiol: Dependence on dose and estrogen receptor subtype. Journal of Neuroscience 29, 5616–5627.

Chu, Z., Moenter, S., 2006. Physiologic regulation of a tetrodotoxin-sensitive sodium influx that mediates a slow afterdepolarization potential in gonadotropin-releasing hormone neurons: possible implications for the central regulation of fertility. Journal of Neuroscience 26, 11961–73.

Conn, P., Freeman, M., 2000. Neuroendocrinology in Physiology and Medicine. Humana Press, 999 Riverview Drive Suite 208 Totowa New Jersey 07512.

Constantin, J., Charles, A., 1999. Spontaneous action potentials initiate rhythmic intercellular calcium waves in immortalized hypothalamic (GT1-1) neurons.

Journal of Neurophysiology 82, 429–435.

Constantin, J., Charles, A., 2001. Modulation of Ca^{2+} signaling by K^+ channels in a hypothalamic neuronal cell line (GT-1). Journal of Neurophysiology 85, 295–304.

Csercsik, D., Szederkényi, G., Hangos, K., Farkas, I., August 12-14 2009a. Dynamical modeling and identification of a GnRH neuron. In: Proceedings of the MCBMS'09 7th IFAC symposium on Modelling and Control in Biomedical Systems. pp. 330–331.

Csercsik, D., Szederkényi, G., Hangos, K., Farkas, I., August 23-26 2009b. Model synthesis and identification of a Hodgkin-Huxley-type GnRH neuron model. In: Proceedings of the ECC'09 European Control Conference. pp. 330–331.

DeFazio, R., Moenter, S., 2002. Estradiol feedback alters potassium currents and firing properties of gonadotropin- releasing hormone neurons. Molecular Endocrinology 16, 2255–2265.

Di Garbo, A., Barbi, M., Chillemi, S., 2007. The synchronization properties of a network of inhibitory interneurons depend on the biophysical model. Biosystems 88, 216–227.

Farkas, I., Varju, P., Liposits, Z., 2007. Estrogen modulates potassium currents and expression of the Kv4.2 subunit in GT1-7 cells. Neurochemistry International 50, 619–627.

Fletcher, P., Li, Y., 2009. An integrated model of electrical spiking, bursting, and calcium oscillations in GnRH neurons. Biophysical Journal 96, 4514–4524.

Gordan, J., Attardi, B., Pfaff, D., 1998. Mathematical exploration of pulsatility in cultured gonadotropin-releasing hormone neurons. Neuroendocrinology 67, 2–17.

Grigoliene, R., Svitra, D., 2000. The mathematical model of the female menstrual cycle and its modifications. Informatica 11, 411–420.

Harris, L., 2001. Differential equation models for the hormonal regulation of the menstrual cycle. PhD thesis, North Carolina State University, www.lib.ncsu.edu/theses/available/etd-04222002-153727/unrestricted/etd.pdf.

Harris, L., Schlosser, P. M., Selgrade, J. F., 2006. Multiple stable periodic solutions in a model for hormonal control of the menstrual cycle. Bulletin of Mathematical Biology 65, 157–173.

Haufler, D., Morin, F., Lacaille, J., Skinner, F., 2007. Parameter estimation in single-compartment neuron models using a synchronization-based method. Neurocomputing 70, 1605–1610.

Helmreich, E., Bakardjieva, A., 1980. Hormonally stimulated adenylate cyclase: A membranous multicomponent system. Biosystems 12, 295–304.

Herbison, A., 2008. Estrogen positive feedback to gonadotropin-releasing hormone (GnRH) neurons in the rodent: The case for the rostral periventricular area of the third ventricle (RP3V). Brain Research Reviews 57, 277–287, doi:10.1016/j.brainresrev.2007.05.006.

Herbison, A., Pape, J., Simonian, S., Skynner, M., Sim, J., 2001. Molecular and cellular properties of GnRH neurons revealed through transgenics in mouse. Molecular and Cellular Endocrinology 185, 185–194.

Hodgkin, A., Huxley, A., 1952. A quantitive description of membrane current and application to conduction and excitation in nerve. Journal of Physiology 117, 500–544.

Hough, P. D., Kolda, T. G., Torczon, V. J., 2000. Asynchronous parallel pattern search for nonlinear optimization. SIAM Journal on Scientific Computing 23, 134–156.

Huys, Q., Ahrens, M., Paninski, L., 2006. Efficient estimation of detailed single-neuron models. Journal of Neurophysiology 96, 872–890, doi:10.1152/jn.00079.2006.

Karsch, F., Cummins, J., Thomas, G., Clarke, I., 1987. Steroid feedback inhibition of pulsatile secretion of gonadotropin-releasing hormone in the ewe. Biology of Reproduction 36, 1207–18.

Kato, M., Ui-Tei, K., Watanabe, M., Sakuma, Y., 2003. Characterization of voltage-gated calcium currents in gonadotropin-releasing hormone neurons tagged with green fluorescent protein in rats. Endocrinology 144, 5118–5125.

Khadra, A., Li, Y., 2006. A model for the pulsatile secretion of gonadotropin-releasing hormone from synchronized hypothalamic neurons. Biophysical Journal 91, 74–83.

Knobil, E., 1980. The neuroendocrine control of the menstrual cycle. Hormone Research 36, 53–88.

Knobil, E., 1988. The hypothalamic gonadotropin hormonr releasing hormone (GnRH) pulse generator in the rhesus monkey and its neuroendocrine control. Human Reproduction 3, 29–31.

Kolda, T., 2005. Revisiting asynchronous parallel pattern search for nonlinear optimization. SIAM J. Optimization 16, 563–586.

Kolda, T., Torczon, V., 2004. On the convergence of asynchronous parallel pattern search. SIAM J. Optimization 14, 939–964.

Komendantov, A., Trayanova, N., Tasker, J., 2007. Somato-dendritic mechanisms underlying the electrophysiological properties of hypothalamic magnocellular neuroendocrine cells: A multicompartmental model study. Journal of Computational Neuroscience 23, 143–168, dOI 10.1007/s1-827-007-0024-z.

Krsmanovic, L., Stojilkovic, S., Merelli, F., Dufour, S., Virmani, M., Catt, K., 1992. Calcium signaling and episodic secretion of gonadotropin-releasing hormone in hypothalamic neurons. Proceedings of the National Academy of Sciences of the USA 89, 8462–8466.

Kuehl-Kovarik, M., K.M.Partin, Handa, R., Dudek, F., 2005. Spike-dependent de-

polarizing afterpotentials contribute to endogenous bursting in gonadotropin releasing hormone neurons. Neuroscience 134, 295–300.

Kusano, K., Fueshko, S., Gainer, H., Wray, S., 1995. Electrical and synaptic properties of embryonic lutenizing hormone-releasing hormone neurons in explant cultures. Proceedings of the National Academy of Sciences of the USA 92, 3918–3992.

LeBeau, A., Goor, F. V., Stojilkovic, S., Sherman, A., 2000. Modeling of membrane excitability in gonadotropin-releasing hormone-secreting hypothalamic neurons regulated by Ca^{2+}-mobilizing and adenylyl cyclase-coupled receptors. The Journal of Neuroscience 20, 9290–9297.

Lee, J., Smaill, B., Smith, N., 2006. Hodgkin-Huxley type ion channel characterization: An improved method of voltage clamp experiment parameter estimation. Journal of Theoretical Biology 242, 123–134.

Luther, J., Tasker, J., 2000. Voltage-gated currents distinguish parvocellular from magnocellular neurones in the rat hypothalamic paraventricular nucleus. Journal of Physiology 523, 193–209.

Maurer, R., Kim, K., Schoderbek, W., Robertson, M., Glenn, D., 1999. Regulation of glycoprotein hormone alpha-subunit gene expression. Recent Progress in Hormone Research 129, 1175–82.

Mellon, P., Windle, J., Goldsmith, P., Padula, C., Roberts, J., Weiner, R., 1990. Immortalization of hypothalamic GnRH neurons by genetically targeted tumorigenesis. Neuron 5, 1–10.

Nunemaker, C., DeFazio, R., Moenter, S., 2003. Calcium current subtypes in GnRH neurons. Biology of Reproduction 69, 1914–1922.

Reinecke, I., Deuflhard, P., 2007. A complex mathematical model of the human menstrual cycle. Journal of Theoretical Biology 247, 303–330.

Roper, P., Callaway, J., Shevchenko, T., Teruyama, R., Armstrong, W., 2003.

AHP's, HAP's and DAP's: How potassium currents regulate the excitability of rat supraoptic neurones. Journal of Computational neuroscience 15, 367–389.

Shorten, P., Wall, D., 2000. A Hodgkin-Huxley model exhibiting bursting oscillations. Bulletin of Mathematical Biology 62, 695–715.

Sim, J., Skynner, M., Herbison, A., 2001. Heterogeneity in the basic membrane properties of postnatal gonadotropin-releasing hormone neurons in the mouse. The Journal of Neuroscience 21, 1067–1075.

Spergel, D., Kruth, U., Hanley, D., Sprengel, R., Seeburg, P., 1999. Gaba- and glutamate-activated channels in green fluorescent protein-tagged gonadotropin-releasing hormone neurons in transgenic mice. The Journal of Neuroscience 19, 2037–2050.

Stojilkovic, S., Krsmanovic, L., Spergel, D., Catt, K., 1994. GnRH neurons: intrinsic pulsatility and receptor-mediated regulation. Trends in Endocrinology and Metabolism 5, 201–209.

Suter, K., Wuarin, J., Smith, B., Dudek, F., Moenter, S., 2000. Whole-cell recordings from preoptic/hypothalamic slices reveal burst firing in gonadotropin-releasing hormone neurons identified with green fluorescent protein in transgenic mice. Endocrinology 141, 3731–3736.

Tabak, J., Murphey, C., Moore, L., 2000. Parameter estimation methods for single neuron models. Journal of Computational Neuroscience 9, 215–236.

Talavera, K., Nilius, B., 2006. Biophysics and structure-function relationship of T-type Ca^{2+} channels. Cell Calcium 40, 97–114.

Tien, J., Guckenheimer, J., 2008. Parameter estimation for bursting neural models. Journal of Computational Neuroscience 24, 358–373, dOI 10.1007/s10827-007-0060-8.

Tien, J., Lyles, D., Zeeman, M., 1996. A potential role of modulating inositol 1,4,5-triphosphate receptor desenzitization and recovery rates in regulating ovulation.

Animal Reproduction Science 42(1-4), 563–570.

Van Goor, F., Krsmanovic, L., Catt, K., Stojilkovic, S., 1999a. Control of action potential-driven calcium influx in GT1 neurons by the activation status of sodium and calcium channels. Molecular Endocrinology 13, 587–603.

Van Goor, F., Krsmanovic, L., Catt, K., Stojilkovic, S., 1999b. Coordinate regulation of gonadotropin-releasing hormone neuronal firing patterns by cytosolic calcium and store depletion. Proceedings of the National Academy of Sciences of the USA 96, 4101–4106.

Van Goor, F., LeBeau, A., Krsmanovic, L., Sherman, A., Catt, K., Stojilkovic, S., 2000. Amplitude-dependent spike-broadening and enhanced Ca^{2+} signaling in GnRH-secreting neurons. Biophysical Journal 79, 1310–1323.

Wang, D., Summers, C., Posner, P., Gelband, C., 1997. A-Type K^+ current in neurons from neonatal rat hypothalamus and brain stem: Modulation by angiotensin II. Journal of Neurophysiology 78, 1021–1029.

Watanabe, M., Sakuma, Y., Kato, M., 2004. High expression of the R-type voltage-gated Ca^{2+} channel and its involvement in Ca^{2+}-dependent gonadotropin-releasing hormone release in GT1-7 cells. Endocrinology 145, 2375–2388.

Wetsel, W., Valença, M., Merchenthaler, I., Liposits, Z., Lópeza, F., Weiner, R., Mellon, P., A.Negro-Villar, 1992. Intrinsic pulsatile secretory activity of immortalized luteinizing hormone-releasing hormone-secreting neurons. Proc. Natl. Acad. Sci. USA 89, 4149–4153.

Williams, C., Thalabard, J., O'Byrne, K., Grosser, P., Nishiara, M., Hotchkiss, J., Knobil, E., 1990. Duration of phasic electrical activity of the hypothalamic gonadotropin-releasing hormone pulse generator and dynamics of luteinizing hormone pulses in the rhesus monkey. Physiology/Pharmacology 87, 8580–8582.

Willms, A., Baro, D., Harris-Warrick, R., Guckenheimer, J., 1999. An improved

parameter estimation method for Hodgkin-Huxley models. Journal of Computational Neuroscience 6, 145–168.

Wilson, R., Kesner, J., Kaufmann, J., Uemura, T., Akema, T., Knobil, E., 1984. Central electrtophsysiological correlates of pulsatile lutenizing hormone secretion in the rhesus monkey. Neuroendocrinology 39, 256–260.

Xu, C., Roepke, T., Zhang, C., Ronnekleiv, O., Kelly, M., 2007. Gonadotropin-releasing hormone (GnRH) activates the M-current in GnRH neurons: An autoregulatory negative feedback mechanism? Endocrinology 149, 2459–2466.

Young, G. D., Keizer, J., 1992. A single-pool inositol 1,4,5-triphosphate-receptor-based model for agonist-stimulated oscillations in $[Ca^{2+}]$ concentration. Proc. Natl. Acad. Sci. 89, 9895–9899.